Thin accretion disk in the Simpson-Visser black-bounce and wormhole spacetimes

Parth Bambhaniya,[1,*] Saurabh,[2,†] Kimet Jusufi,[3,‡] and Pankaj S. Joshi[1,§]

[1]*International Center for Cosmology, Charusat University, Anand, GUJ 388421, India*
[2]*P. D. Patel Institute of Applied Sciences, Charusat University, Anand, 388421 Gujarat, India*
[3]*Physics Department, State University of Tetovo, Ilinden Street nn, 1200 Tetovo, North Macedonia*

(Received 2 October 2021; accepted 6 January 2022; published 21 January 2022)

We compare the optical appearance of a thin accretion disk in the Simpson-Visser spacetime to the Schwarzschild black hole case in this paper. We calculate and illustrate the redshift and observed flux distributions as viewed by distant observers at various inclination angles. Simpson-Visser family of metrics creates Novikov-Thorne (NT) accretion disks images that nearly look like a Schwarzschild black hole's NT accretion disk. We have studied also the embedding diagram, the electromagnetic properties of the accretion disk such as the temperature and the radiation flux of the energy by the accretion disk and the accretion efficiency. Compared to the Schwarzschild black hole, we find that the temperature, radiation flux of the energy, and the luminosity of the accretion disk increase by increasing the regularization parameter l. We conclude that, based on astrophysical observational signatures in the properties of the electromagnetic spectrum, we can distinguish the wormhole geometries from the regular black holes (black-bounce) and the Schwarzschild black hole.

DOI: 10.1103/PhysRevD.105.023021

I. INTRODUCTION

Black holes are arguably the most fascinating predictions of Einstein's general theory of relativity. It is now evident that both astronomical observations and the theoretical formulation of general relativity suggest their real existence in nature. The most striking evidence for their existence is the detection of the gravitational waves [1] and the shadow image of the supermassive M87* [2,3]. Black holes are extremely important in explaining many other problems in astrophysics that have to do with the high-energy phenomena in the form of x-ray emission and jets, accretion of matter, quasi-periodic oscillations, and the motions of nearby objects in orbit around the hidden mass [4].

Despite all these successes, there are still some conceptual problems related to black holes in general relativity. More specifically, the main problem associated with black holes is the existence of singularities at the coordinate center. As of today, this problem has not been solved. Many physicists have speculated that a quantum theory of gravity can solve this problem. However, the phenomenology of black holes remains a hot topic after the EHT findings. The black hole mimickers such as regular black holes, wormholes, naked singularities, grava-stars, etc., are also growing significantly in the literature [5–13].

The concept of a regular black hole was first introduced by Bardeen in 1968 [14] (see also the more recent references [15–26]), and it has been intuitively interesting due to its nonsingular structure. One motivation for exploring such compact objects is that they could be black hole alternatives. Furthermore, as is widely known, many of the possible observational signatures of the black holes such as precession of timelike bound orbits, gravitational lensing, and shadow properties can be mimicked by black hole mimickers [27–36].

From a historical perspective, it's worth noting that Einstein and Rosen proposed the existence of "bridges" through spacetime [37] using the theory of general relativity. These bridges connect two places in spacetime, allowing for the creation of Einstein-Rosen bridges, also known as wormholes. Such wormholes have been proved to be nontraversable. The notion of having traversable wormholes was later investigated in the pioneering work of Morris and Throne [38].

The exotic matter that satisfies the flare-out criterion and violates the weak energy condition is required to sustain the structure of a wormhole (see [38,39]). However, quantum matter fields have recently been proved to provide enough negative energy to allow some wormholes to be traversed. As a result, an exotic matter with negative energy density and large negative pressure, with a greater value than the energy density, is required to form such a traversable wormhole [40,41].

*grcollapse@gmail.com
†sbhkmr1999@gmail.com
‡kimet.jusufi@unite.edu.mk
§psjcosmos@gmail.com

We can therefore try to test black holes and wormholes using astrophysical data. In Ref. [42], authors studied the possibility to test wormhole geometries in our galaxy using infalling and radiating gas accretion model and the motion of the S2 star. The possibility of testing wormholes by observing the Galactic Center using the infalling gas model was studied in Refs. [43,44]. Other interesting works concerning the formation and the stability of wormholes can be found in Refs. [45–47]. Based on astrophysical observations, today we know that in the Galactic Center of many galaxies, a disk is formed. Namely, such a disk is made of rapidly rotating gas that slowly spirals onto a compact body, which is assumed to be a black hole. During such accretion, the gravitational energy through the friction of the heat converts into radiation, which partially escapes, and cools down the accretion disk. The only information that we have about accretion disk physics comes from this radiation, when it reaches radio, optical, and x-ray telescopes, allowing astronomers to analyze its electromagnetic spectrum and its time variability. The radiation properties of thin accretion disks were further analyzed in the recent papers [48–54], where the effects of photon capture by the black hole on the spin evolution were presented as well.

Simpson and Visser proposed a very simple theoretically appealing spherically symmetric and static spacetime family [55], derived from Schwarzschild geometry, that allows for a unique description of regular black hole and wormholes by smooth interpolation between these two possibilities using a length-scale parameter l that drives the regularization of the central singularity. Its rotational form was recently shown as well [56]. In the present work, we are interested to use the Simpson and Visser metric and explore the NT accretion disk properties and images. It will be interesting to see whether or not we can distinguish the regular and nonregular black hole from the wormhole case. This metric is of particular interest since it can describe a regular or nonregular black hole or traversable wormhole depending on the value of the regularization parameter l. Note that many physical properties of this metric, including the effect of charge, gravitational lensing, quasi-normal modes, and other effects were studied by many authors [57–64]. In the present work, we are interested to study the optical appearance and the electromagnetic properties of the NT accretion disk around the Simpson-Visser metric.

This paper is organized as follows. In Sec. II, we present the Simpson-Visser metric. In Sec. III, we study the embedding diagram. In Sec. IV, we study the NT accretion disk and the images. In Sec. V, we explore the electromagnetic properties of the accretion disk. Finally, in Sec. VI, we comment on our results. Throughout this paper, we consider gravitational constant (G) and speed of light (c) as unity.

II. SIMPSON-VISSER SPACETIME

The proposed spherically symmetric and static Simpson-Visser metric specifies a class of black hole mimickers with a minimal surface in place of the central singularity. The geometry of spacetime is given by [55]

$$ds^2 = -f(r)dt^2 + \frac{dr^2}{f(r)} + (r^2 + l^2)(d\theta^2 + \sin^2\theta d\phi^2), \tag{2.1}$$

where,

$$f(r) = \left(1 - \frac{2M}{\sqrt{r^2 + l^2}}\right). \tag{2.2}$$

In the above spacetime, $M \geq 0$ represents the ADM mass, and $l > 0$ is a parameter responsible for the regularization of the central singularity and possibly reflecting the quantum gravity effects. The above spacetime (2.1) neatly interpolates between the standard Schwarzschild black hole and the Morris-Thorne traversable wormhole: passing through a black-bounce (into a future incarnation of the universe), an extremal null-bounce (into a future incarnation of the universe), and a traversable wormhole are all intermediary stages. Therefore, this spacetime consists of a family of solutions as the black hole mimickers, which can be described as

(1) The ordinary Schwarzschild spacetime ($l = 0$),
(2) A "black-bounce" (regular black hole) with a one-way spacelike throat ($l < 2M$),
(3) A one-way wormhole with a null throat ($l = 2M$),
(4) A traversable wormhole in the Morris–Thorne sense ($l > 2M$).

The Simpson and Visser metric is everywhere regular as long as the parameter l is nonzero, resulting in an unusual kind of "regular black hole," where the "origin" at $r = 0$ can be spacelike, null, or timelike. Moreover, the CarterPenrose diagrams and curvature tensors are defined in [55] and shown that the Einstein tensor has nonzero (mixed) components. In the present work, we are interested to understand the effect of l on the physical properties of the electromagnetic waves emitted by the accretion disk.

III. EMBEDDING DIAGRAM

Let us study the geometry of the Simpson-Visser metric by embedding it into a higher-dimensional Euclidean space. To simplify the problem, let us consider the equatorial plane $\theta = \pi/2$ at a fixed moment $t =$ Constant, in that case, we have

$$ds^2 = \frac{dr^2}{1 - \frac{b(r)}{r}} + \mathcal{R}^2 d\phi^2, \tag{3.1}$$

where

$$b(r) = r(1 - f(r)), \qquad \mathcal{R}^2 = r^2 + l^2. \tag{3.2}$$

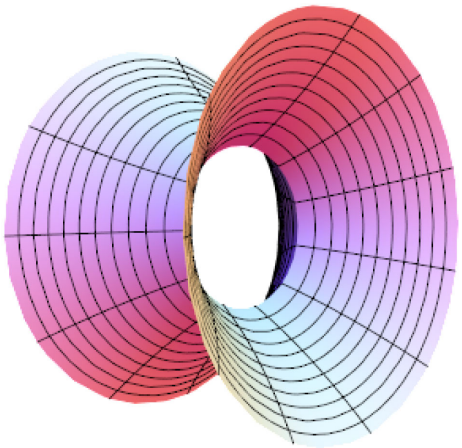

FIG. 1. The geometry of Simpson-Visser wormhole embedded in a three-dimensional Euclidean space. We have used $l = 2.1$ and $M = 1$.

Let us embed this black hole metric into three-dimensional Euclidean space in the cylindrical coordinates,

$$ds^2 = dz^2 + d\mathcal{R}^2 + \mathcal{R}^2 d\phi^2, \tag{3.3}$$

which can be written as follows:

$$ds^2 = \left[\left(\frac{d\mathcal{R}}{dr}\right)^2 + \left(\frac{dz}{dr}\right)^2\right] dr^2 + \mathcal{R}^2 d\phi^2. \tag{3.4}$$

From these equations, we find that

$$\frac{dz}{dr} = \pm\sqrt{\frac{r}{r - b(r)} - \left(\frac{d\mathcal{R}}{dr}\right)^2}. \tag{3.5}$$

As a particular case, we will consider the traversable wormhole with $l > 2$. Note that the integration of the last expression cannot be accomplished analytically. Invoking numerical techniques allows us to illustrate the embedding diagrams for the Simpson-Visser traversable wormhole given in Fig. (1).

IV. NOVIKON-THORNE THIN ACCRETION DISKS

Massive particles move in stable circular timelike geodesics in the geometrically thin accretion disk. The Novikov-Thorne model of a thin accretion disk is considered here. There are two constants of motion along the timelike geodesics because we are dealing with spherically symmetric and static spacetimes. The particles' energy $(\tilde{E})$ and angular momentum $(\tilde{L})$ per unit rest mass are represented as

$$\tilde{E} = \left(1 - \frac{2M}{\sqrt{r^2 + l^2}}\right)\dot{t}, \qquad \tilde{L} = (r^2 + l^2)\dot{\phi}, \tag{4.1}$$

where the over dot represents the derivative with respect to proper time (τ). Using the above conserved quantities and timelike geodesic condition $(ds^2 = -m^2)$, we can write the general form of spherically symmetric and static spacetime (2.1) as

$$\tilde{E}^2 = \dot{r}^2 + V_{\text{eff}}(r). \tag{4.2}$$

This above equation represents the total energy of the particle, where $V_{\text{eff}}(r)$ is the effective potential of the Simpson-Visser spacetime for timelike geodesics. The effective potential of the Simpson-Visser spacetime is defined as

$$V_{\text{eff}}(r) = \tilde{L}^2 \frac{\left(1 - \frac{2M}{\sqrt{r^2+l^2}}\right)}{(r^2 + l^2)} + \left(1 - \frac{2M}{\sqrt{r^2 + l^2}}\right) m^2, \tag{4.3}$$

where, for photons, $m = 0$ and for test particles, $m > 0$ (see Fig. 2). The sign of the circular geodesic orbits determines their stability. The condition $V''_{\text{eff}}(r_c) = 0$ determines the marginally innermost stable circular orbit (ISCO). It indicates the ISCO position at the radius,

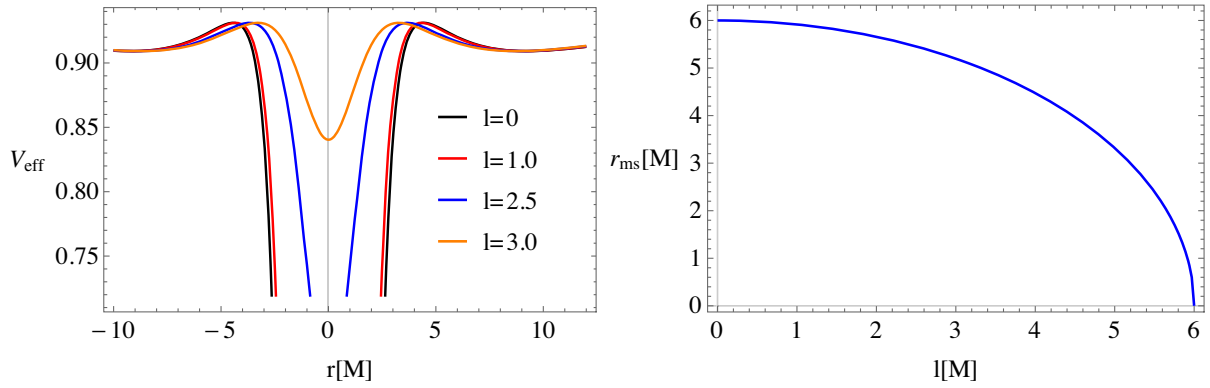

FIG. 2. Left panel: The effective potential for different values of l and $M = 1$. Right panel: The radius of the marginally stable circular orbit or the ISCO for different values of l and $M = 1$.

$$r_{\rm ISCO} = \sqrt{(6M)^2 - l^2}. \tag{4.4}$$

The horizon position of a regular black hole ($l < 2M$) is defined as

$$r_h = \sqrt{(2M)^2 - l^2}. \tag{4.5}$$

For the shadow size, one can calculate the radius of the circular orbit of a photon ($l < 3M, ds^2 = 0$) as

$$r_{\rm ph} = \sqrt{(3M)^2 - l^2}, \tag{4.6}$$

and the critical impact parameter $b = E/L$ of the photon circular orbits is given by the expression,

$$b_{\rm ph}^2 = 27M^2, \tag{4.7}$$

having the same size as a photon circular orbit around a Schwarzschild black hole, and does not depend on l [63]. Note that for $l > 3M$, there is no photon sphere, but we have a contribution from the wormhole throat. Now, the stable circular timelike geodesic can be obtained by satisfying the conditions,

$$V_{\rm eff}(r) = \tilde{E}^2, \qquad V'_{\rm eff}(r) = 0, \qquad V''_{\rm eff}(r) < 0, \tag{4.8}$$

where the first two conditions are useful to get $\tilde{E}$ and $\tilde{L}$ as a function of radius of the circular orbit as

$$\tilde{E} = \frac{1 - \frac{2M}{\sqrt{r^2+l^2}}}{\sqrt{1 - \frac{2M}{\sqrt{r^2+l^2}} - (r^2+l^2)\Omega^2}}, \tag{4.9}$$

$$\tilde{L} = \frac{(r^2+l^2)\sqrt{\frac{M}{(r^2+l^2)^{3/2}}}}{\sqrt{1 - \frac{2M}{\sqrt{r^2+l^2}} - (r^2+l^2)\Omega^2}}, \tag{4.10}$$

where Ω gives the angular momentum of the particles in terms of the equation [48],

$$\Omega = \frac{d\phi}{dt} = \sqrt{\frac{f'(r)}{2r}} = \sqrt{\frac{M}{(r^2+l^2)^{3/2}}}, \tag{4.11}$$

with prime representing a derivative with respect to the radial coordinate r. For more details about the properties of the circular geodesic motion, see [65].

In this part, we use the Novikov-Thorne model of a thin accretion disk composed of anisotropic fluid moving in the equatorial plane to examine the steady-state thin accretion disk. Certain structure equations govern the physical properties of the accretion disk, which arises from the necessity of the fluid's rest mass, energy, and angular momentum conservation. In this setup, the accreting matter in the disk can be described by the stress-energy tensor given by [49]

$$T^{\mu\nu} = \rho_0 u^\mu u^\nu + 2u^{(\mu}q^{\nu)} + t^{\mu\nu}, \tag{4.12}$$

where

$$u_\mu q^\mu = 0, \tag{4.13}$$

$$u_\mu t^{\mu\nu} = 0. \tag{4.14}$$

In the above equations, we have the introduced the following quantities: ρ_0, q^μ, and $t^{\mu\nu}$, which are known as the rest mass density of the accreting matter, the energy flow vector, and the stress tensor, respectively. These quantities are specified in the averaged rest-frame of the particle described by the four-velocity u^μ. If the rest mass is conserved, the equation can be used as

$$\nabla_\mu(\rho_0 u^\mu) = 0. \tag{4.15}$$

As a result, the disk radius has no effect on the time-averaged rate of rest mass accretion,

$$\dot{M}_0 = -2\pi\sqrt{-g}\Sigma u^r = \text{const.}, \tag{4.16}$$

where $\Sigma(r)$ denotes the time-averaged surface density in cylindrical coordinates, and

$$\Sigma(r) = \int_{-H}^{H} < \rho_0 > dz. \tag{4.17}$$

The law of energy conservation and the law of angular momentum conservation both state that

$$\nabla_\mu T^{t\mu} = 0, \tag{4.18}$$

$$\nabla_\mu T^{\phi\mu} = 0. \tag{4.19}$$

These relationships can be used to obtain the thin disk's time-averaged radial structure equations,

$$[\dot{M}_0\tilde{E} - 2\pi\sqrt{-g}\Omega W^r_\phi]_{,r} = 4\pi r F(r)\tilde{E}, \tag{4.20}$$

and

$$[\dot{M}_0\tilde{L} - 2\pi\sqrt{-g}W^r_\phi]_{,r} = 4\pi r F(r)\tilde{L}, \tag{4.21}$$

where W^r_ϕ is the averaged torque and is given by

$$W^r_\phi = \int_{-H}^{H} < t^r_\phi > dz. \tag{4.22}$$

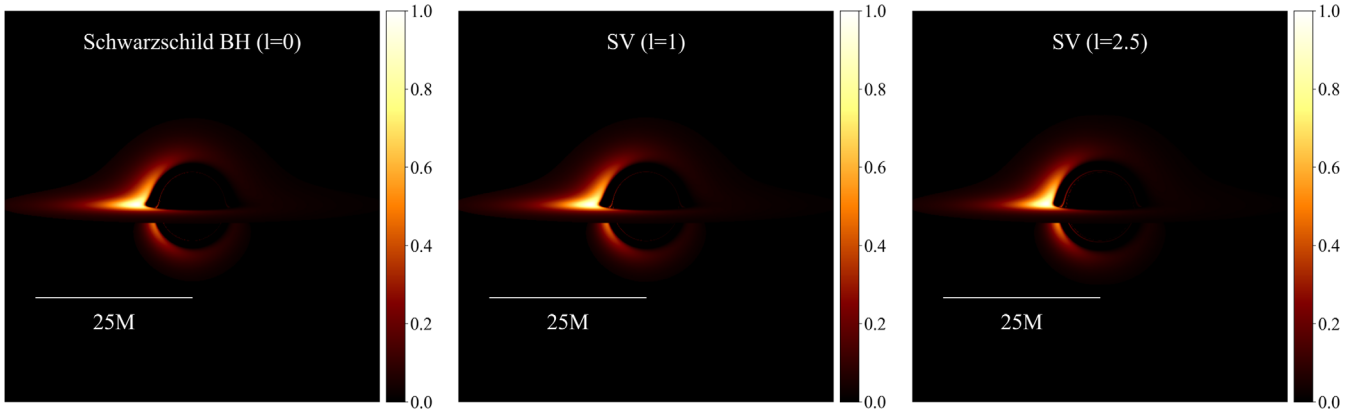

FIG. 3. Images of the Novikov-Thorne thin-accretion disk around Schwarzschild black hole and Simpson-Visser regular black hole with $l = 1$ and wormhole with $l = 2.5$ for inclination 90°.

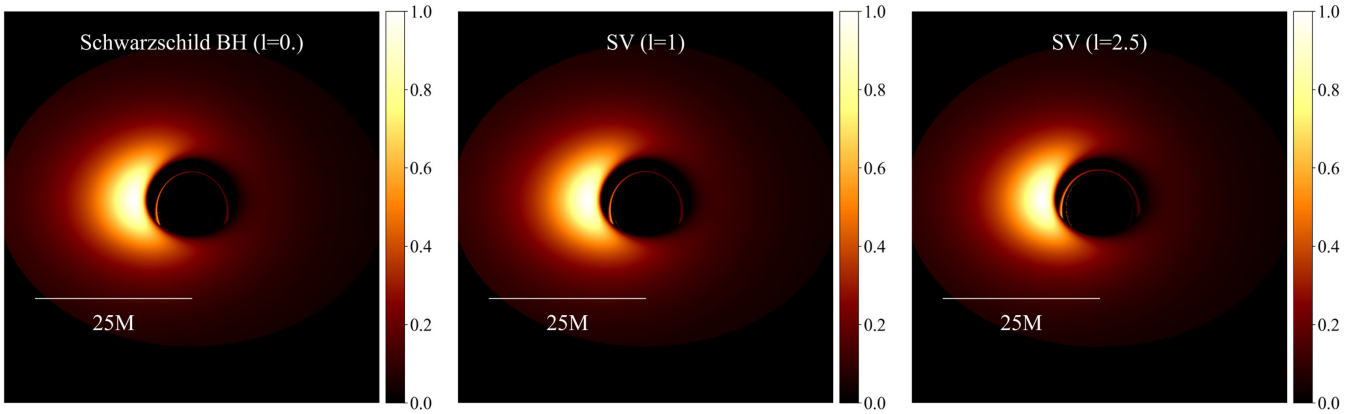

FIG. 4. Images of the Novikov-Thorne thin-accretion disk around Schwarzschild Black hole and Simpson-Visser regular black hole with $l = 1$ and wormhole with $l = 2.5$ for inclination 45°.

At this point, it's important to emphasize that the $\phi - r$ component of the stress tensor averaged over a characteristic time scale Δt and the azimuthal angle $\Delta\phi = 2\pi$ is the quantity $< t^r_\phi >$. The flux $F(r)$ of the radiant energy over the disk can be represented in terms of the specific energy, angular momentum, and angular velocity of the orbiting particle in the thin accretion by using the energy-angular momentum relation, $\tilde{E}_{,r} = \omega\tilde{L}_{,r}$. The flux of electromagnetic radiation emitted from a radial position r of a disk is given by the standard formula, which may be deduced from the equations (4.9), (4.10), and (4.11) [48],

$$F(r) = -\frac{\dot{M}}{4\pi\sqrt{-g}}\frac{\Omega'}{(\tilde{E}-\Omega\tilde{L})^2}\int_{r_{\rm in}}^{r}(\tilde{E}-\Omega\tilde{L})\tilde{L}'dr. \qquad (4.23)$$

Note that $r_{\rm in}$ represents the inner edge of the disk, and $\dot{M}$ is the mass accretion rate. In Figs. 3 and 4, we show the optical appearance of the Simpson-Visser spacetime surrounded by NT accretion disk. We use the ray-tracing formalism described in [65] to numerically integrate the geodesic equation using `RK45` method with adaptive step size. In Fig. 5, we show the horizontal cross-sectional intensity for different values of l and highlight the peak intensity for the same. One can see that the images are

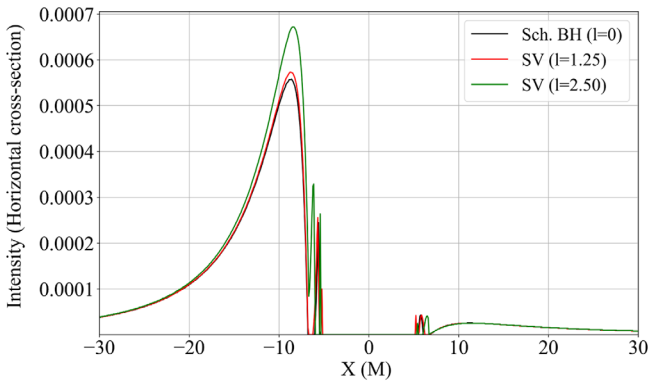

FIG. 5. The plot shows the horizontal cross-sectional intensity of the Novikov-Thorne accretion disks for $l = 0$ and $l = 1.25$, respectively.

almost similar compared to the Schwarzschild geometry, which makes it difficult to distinguish these two spacetime geometries. However, in what follows, we shall study in more details this problem; in particular, we shall study in the electromagnetic properties of the Simpson-Visser spacetime and compare to the Schwarzschild geometry.

V. THE RADIATING FLUX, TEMPERATURE PROFILE, AND THE LUMINOSITY OF THIN ACCRETION DISK

In this section, we turn our attention to explore in more details the electromagnetic properties of the accretion disk, such as the radiation flux $F(r)$, the temperature profile, luminosity, and the accretion efficiency. Toward this purpose, we will numerically analyze the behavior of the above quantities with respect to the parameter l. Furthermore, we assume a central compact object with mass $M = 10^6\ M_\odot$ (a supermassive black hole), along two cases for the accretion rate given as follows [49,54]:

$$\dot{M}_0 \sim 10^{-5}\ M_\odot/\mathrm{yr} \quad \text{and} \quad \dot{M}_0 \sim 10^{-12}\ M_\odot/\mathrm{yr}. \tag{5.1}$$

Recall that the radiation flux $F(r)$ given by Eq. (4.23) represents the emitted flux by the thin accretion disk in the Simpson-Visser spacetime. Moreover, we expect that the Stefan-Boltzmann law holds, and therefore, in terms of the effective temperature associated to the accretion disk, we have

$$T_{\mathrm{eff}}(r) = \left(\frac{F(r)}{\sigma}\right)^{1/4}, \tag{5.2}$$

where, for the Stefan-Boltzmann constant, we have $\sigma = 5.67 \times 10^{-5}\ \mathrm{erg\,s^{-1}\,cm^{-2}}\,K^{-4}$. Our analyses shows that the temperature and the radiated energy flux of the disk increases by increasing the parameter l, as can be seen from Figs. 6 and 7. As a specific example, take the case $\dot{M}_0 \sim 8 \times 10^{-12}\ M_\odot/\mathrm{yr}$; we find that the maximal value for the temperature at a particular l occurs at

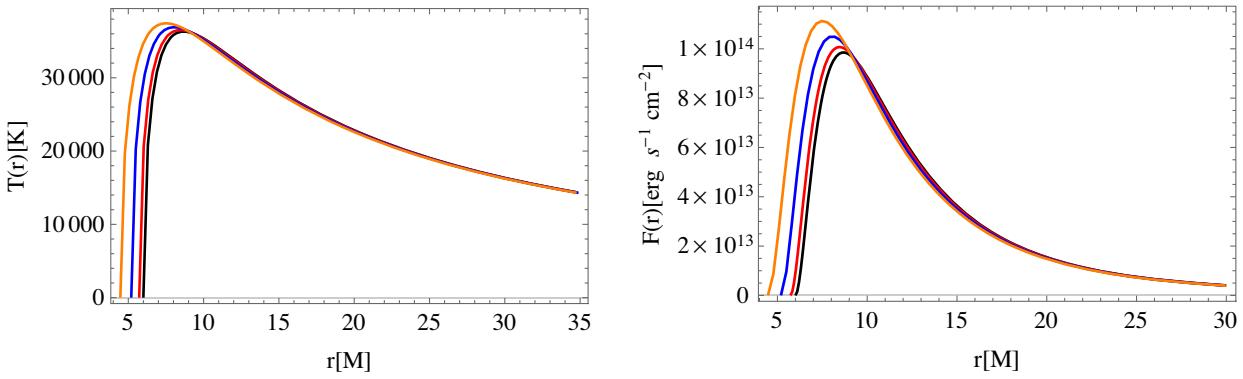

FIG. 6. Left panel: The temperature profile of the thin accretion disk for different values of l using the case $M = 10^6 M_0$ and $\dot{M}_0 \sim 2.5 \times 10^{-5}\ M_\odot/\mathrm{yr}$. Right panel: The radiated energy flux over the thin accretion disk for different values of l and $M = 1$. In both plots, we have $l = 0$ (black curve), $l = 1.8$ (red curve), $l = 3.0$ (blue curve), and $l = 4.0$ (orange curve).

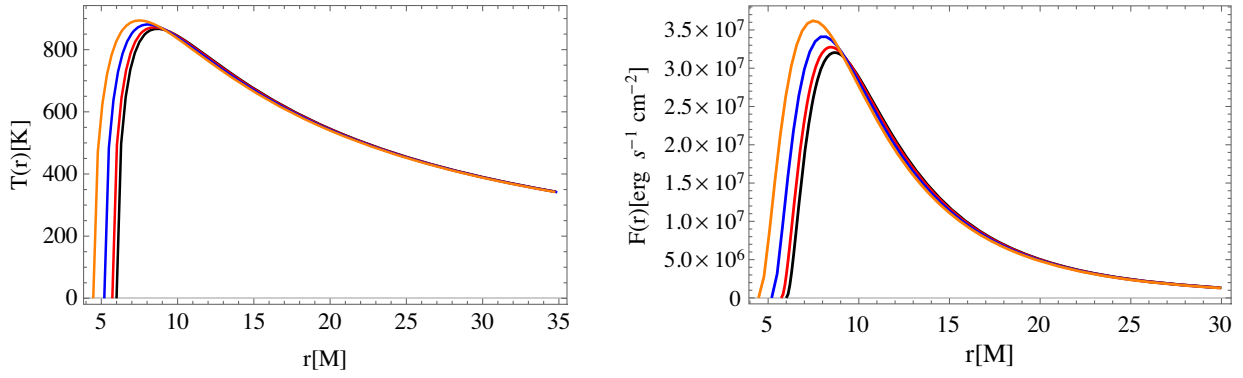

FIG. 7. Left panel: The temperature profile of the thin accretion disk for different values of l using the case $M = 10^6 M_0$ and $\dot{M}_0 \sim 8 \times 10^{-12}\ M_\odot/\mathrm{yr}$. Right panel: The radiated energy flux over the thin accretion disk for different values of l and $M = 1$. In both plots, we have $l = 0$ (black curve), $l = 1.8$ (red curve), $l = 3.0$ (blue curve), and $l = 4.0$ (orange curve) in both plots.

$$l = 0.0 : T_{\max} \simeq 867.01 \text{ K}, \qquad r = 8.70[M],$$

$$l = 1.8 : T_{\max} \simeq 871.79 \text{ K}, \qquad r = 8.42[M],$$

$$l = 3.0 : T_{\max} \simeq 881.04 \text{ K} \qquad r = 8.09[M].$$

On the other hand, the maximal value for the radiating flux at particular l occurs at

$$l = 0.0 : F_{\max} \simeq 3.203 \times 10^{7}\, \text{erg}\, \text{s}^{-1}\, \text{cm}^{-2}, \quad r = 8.70[M],$$

$$l = 1.8 : F_{\max} \simeq 3.275 \times 10^{7}\, \text{erg}\, \text{s}^{-1}\, \text{cm}^{-2}, \quad r = 8.42[M],$$

$$l = 3.0 : F_{\max} \simeq 3.416 \times 10^{7}\, \text{erg}\, \text{s}^{-1}\, \text{cm}^{-2}, \quad r = 8.09[M].$$

The observed luminosity $L(\nu)$ of the thin accretion disk around the Simpson-Visser spacetime has a redshifted black body spectrum, while we assume the radiation emitted by the thin accretion disk surface to be perfect black body radiation [49],

$$L(\nu) = 4\pi d^2 I(\nu), \tag{5.3}$$

or

$$L(\nu) = \frac{8\pi h \cos i}{c^2} \int_{r_i}^{r_f} \int_{0}^{2\pi} \frac{\nu_e^3 r d\phi dr}{\exp(\frac{h\nu_e}{k_B T}) - 1}. \tag{5.4}$$

In this equation, i is the thin accretion disk's inclination angle around the black hole, while d is the distance between the observer and the center of the thin accretion disk, along with the Planck constant h, emission frequency ν_e, as well as the Boltzmann constant k_B. Furthermore, we need to find the redshift factor, which can be found from

$$g = \frac{\nu}{\nu_e} = \frac{k_\mu u_o^\mu}{k_\mu u_e^\mu}, \tag{5.5}$$

where ν is the radiation frequency in the faraway observer's local rest frame. We also have the observer's four-velocity,

$$u_o^\mu = (1, 0, 0, 0), \tag{5.6}$$

and the four-velocity of the emitter,

$$u_e^\mu = (u_e^t, 0, 0, \Omega u_e^t). \tag{5.7}$$

We can take $r_i = r_{\text{ms}}$ and r_f to any arbitrary large distance from the compact object. To illustrate the effect and see how the parameter l affects the emission spectrum, we calculate the radiation spectrum $\nu L(\nu)$ numerically. We find that with the increase of the parameter l for both accretion rates, the observed luminosity increases as shown in Fig. 8. If we take the accretion case dot $M_0 \sim 8 \times 10^{-5}\ M_\odot/\text{yr}$, we find that the maximal value for the luminosity at particular l occurs at the frequency $\nu = 4.33 \times 10^{13}$ Hz along with the following values for the luminosity,

$$l = 0.0 : \nu L_{\max} \simeq 1.158 \times 10^{33} \text{ erg}\, \text{s}^{-1},$$

$$l = 1.8 : \nu L_{\max} \simeq 1.169 \times 10^{33} \text{ erg}\, \text{s}^{-1},$$

$$l = 3.0 : \nu L_{\max} \simeq 1.188 \times 10^{33} \text{ erg}\, \text{s}^{-1}.$$

Finally, we can think about accretion efficiency, which is calculated as the ratio of the rate of photons escaping from the disk surface to infinity compared to the rate of mass-energy transport to the black hole. There is a simple way to estimate the efficiency ϵ of the accretion disk since it can be found to be proportional to the specific energy of the

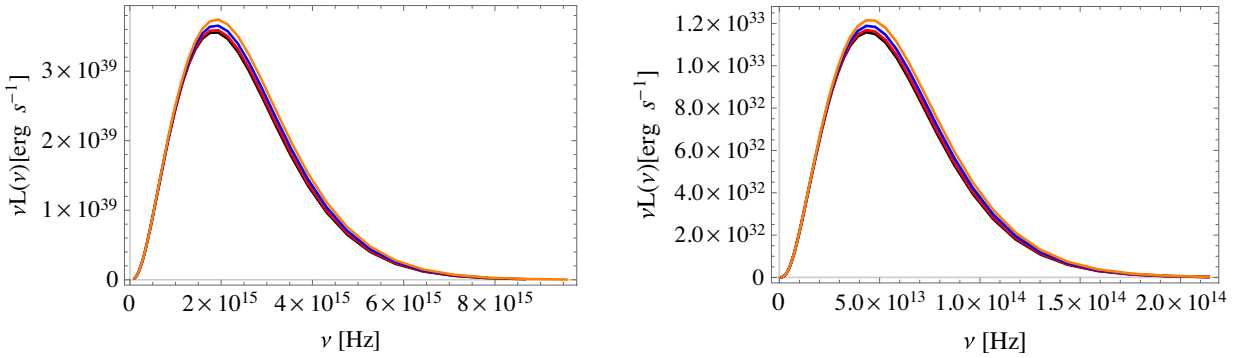

FIG. 8. Left panel: The observed luminosity of the thin accretion disk for different values of l using the case $M = 10^6 M_0$ and $\dot{M}_0 \sim 2.5 \times 10^{-5}\ M_\odot/\text{yr}$. Right panel: The observed luminosity of the thin accretion disk for different values of l using the case $M = 10^6 M_0$ and $\dot{M}_0 \sim 8 \times 10^{-12}\ M_\odot/\text{yr}$. We have $l = 0$ (black curve), $l = 1.8$ (red curve), $l = 3.0$ (blue curve), and $l = 4.0$ (orange curve) in both plots.

moving particle in the disk, as measured at the marginally stable orbit by

$$\epsilon = 1 - \tilde{E}_{\rm ms}. \tag{5.8}$$

Interestingly, for the efficiency of the accretion disk in the Simpson-Visser spacetime, we find that this quantity is not affected by the parameter l, and it is given by

$$\epsilon = \frac{3 - 2\sqrt{2}}{3} \simeq 0.0571909588. \tag{5.9}$$

Although the radiating energy changes, we found that based on the accretion efficiency ϵ, one cannot distinguish the Simpson-Visser metric from the Schwarzschild geometry. This quantity is important and provides information about the efficient engine, in our case, the accretion disk, for converting accreting matter's energy into electromagnetic radiation. It's interesting to see that this quantity remains constant and does not depend on the parameter l. From the plot of luminosity as a function of the frequency of the emitted electromagnetic waves from the accretion disk, we saw that it depends on the spacetime geometry. This, in turn, allows one to distinguish different spacetime geometries. In addition, the observed luminosity depends on the accretion mass rate. That means that in order to constrain a given solution, we need a precise value for the accretion mass rate for a given source and observational data for the luminosity, which may be obtained by means of other astrophysical observations (here, we have used two examples of the mass accretion rate). With this information in hand, we can compare and test different geometries. Another quantity of interest is the radiation energy flux, which also encodes information about the spacetime geometry. In this direction, we point out a similar method based on the thermal radiation used by Bambi [66] to analyze the photon flux number density as measured by a distant observer to test the nature of the black hole and modified gravity. In addition, the so-called continuum-fitting method has been used, for example, in Ref. [67] to constrain different geometries.

VI. CONCLUSIONS

The Simpson-Visser model has the additional benefit of analytically smoothly shifting from black holes (singular or regular) to wormholes (one-way or traversable). In some ways, the regular black hole shown above in this paper is, in fact, the conventional Schwarzschild solution for $l = 0$. This is a clear contrast to the scenario in which a collapsing regular black hole bounces back into our own universe, and it is a situation worth considering in its own right. It'll be interesting to see if we can tell the difference between a regular and singular black hole and a wormhole. This metric is particularly interesting because, depending on the value of the regularization parameter l, it can either describe a regular or singular black hole or a traversable or one-way wormhole. Therefore, in this paper, we studied the optical appearance of a thin accretion disk in the Simpson-Visser spacetime. We calculated and illustrated the observed flux distributions as viewed by a distant observer. The image generated in the Simpson-Visser metric looks similar to that of Schwarzschild. In addition, we studied the electromagnetic properties of the accretion disk such as the temperature and the radiation flux of the energy by the accretion disk. It is shown that by increasing the regularized parameter l, the temperature, as well as the radiating flux, increases, compared to the Schwarzschild geometry. Thus, for these solutions, we conclude that the specific signatures that appear in the electromagnetic spectrum lead to the possibility of distinguishing wormhole geometries from the Schwarzschild solution by using astrophysical observations of the emission spectra from accretion disks. As an interesting result, we show that the accretion efficiency remains constant and does not depend on l. In the near future, we plan to use astrophysical data to constrain the regularized parameter l.

[1] B. P. Abbott *et al.* (LIGO Scientific and Virgo Collaborations), Phys. Rev. Lett. **116**, 061102 (2016).
[2] K. Akiyama *et al.* (Event Horizon Telescope Collaboration), Astrophys. J. **875**, L1 (2019).
[3] K. Akiyama *et al.* (Event Horizon Telescope Collaboration), Astrophys. J. **875**, L4 (2019).
[4] R. Abuter *et al.* (GRAVITY Collaboration), Astron. Astrophys. **636**, L5 (2020).
[5] S. A. Hayward, Phys. Rev. Lett. **96**, 031103 (2006).
[6] M. Visser and D. L. Wiltshire, Classical Quantum Gravity **21**, 1135 (2004).
[7] P. S. Joshi and I. H. Dwivedi, Phys. Rev. D **47**, 5357 (1993).
[8] P. Gao, D. L. Jafferis, and A. C. Wall, J. High Energy Phys. 12 (2017) 151.
[9] K. Mosani, D. Dey, and P. S. Joshi, Phys. Rev. D **101**, 044052 (2020).
[10] K. Mosani, D. Dey, and P. S. Joshi, Phys. Rev. D **102**, 044037 (2020).
[11] K. Mosani, D. Dey, and P. S. Joshi, Mon. Not. R. Astron. Soc. **504**, 4743 (2021).
[12] M. Azreg-Aïnou, J. Cosmol. Astropart. Phys. 07 (2015) 037.
[13] M. Amir, K. Jusufi, A. Banerjee, and S. Hansraj, Classical Quantum Gravity **36**, 215007 (2019).

[14] J. M. Bardeen, nonsingular general-relativistic gravitational collapse, in *Proceedings of the International Conference GR5, 1968* (USSR, Tbilisi, 1968), p. 174.
[15] Thomas A. Roman and Peter G. Bergmann, Phys. Rev. D **28**, 1265 (1983).
[16] S. A. Hayward, Phys. Rev. Lett. **96**, 031103 (2006).
[17] J. M. Bardeen, arXiv:1406.4098.
[18] V. P. Frolov, J. High Energy Phys. 05 (2014) 049.
[19] V. P. Frolov, arXiv:1411.6981.
[20] V. P. Frolov, Phys. Rev. D **94**, 104056 (2016).
[21] V. P. Frolov and A. Zelnikov, Phys. Rev. D **95**, 124028 (2017).
[22] V. P. Frolov, EPJ Web Conf. **168**, 01001 (2018).
[23] P. A. Cano, S. Chimento, T. Ortín, and A. Ruipérez, Phys. Rev. D **99**, 046014 (2019).
[24] J. M. Bardeen, arXiv:1811.06683.
[25] R. Carballo-Rubio, F. Di Filippo, S. Liberati, C. Pacilio, and M. Visser, J. High Energy Phys. 07 (2018) 023.
[26] R. Carballo-Rubio, F. Di Filippo, S. Liberati, and M. Visser, Phys. Rev. D **98**, 124009 (2018).
[27] P. Bambhaniya, A. B. Joshi, D. Dey, and P. S. Joshi, Phys. Rev. D **100**, 124020 (2019).
[28] A. B. Joshi, P. Bambhaniya, D. Dey, and P. S. Joshi, arXiv:1909.08873.
[29] P. Bambhaniya, D. N. Solanki, D. Dey, A. B. Joshi, P. S. Joshi, and V. Patel, Eur. Phys. J. C **81**, 205 (2021).
[30] P. Bambhaniya, D. Dey, A. B. Joshi, P. S. Joshi, D. N. Solanki, and A. Mehta, Phys. Rev. D **103**, 084005 (2021).
[31] S. Nampalliwar, S. Kumar, K. Jusufi, Q. Wu, M. Jamil, and P. Salucci, Astrophys. J. **916**, 116 (2021).
[32] K. Jusufi and Saurabh, Mon. Not. R. Astron. Soc. **503**, 1310 (2021).
[33] K. Saurabh and K. Jusufi, Eur. Phys. J. C **81**, 490 (2021).
[34] S. Nampalliwar and S. K., arXiv:2108.01190.
[35] A. B. Joshi, D. Dey, P. S. Joshi, and P. Bambhaniya, Phys. Rev. D **102**, 024022 (2020).
[36] D. Dey, P. S. Joshi, A. Joshi, and P. Bambhaniya, Int. J. Mod. Phys. D **28**, 1930024 (2019).
[37] A. Einstein and N. Rosen, Phys. Rev. **48**, 73 (1935).
[38] M. S. Morris and K. S. Thorne, Am. J. Phys. **56**, 395 (1988).
[39] M. S. Morris, K. S. Thorne, and U. Yurtsever, Phys. Rev. Lett. **61**, 1446 (1988).
[40] K. Jusufi, A. Banerjee, and S. G. Ghosh, Eur. Phys. J. C **80**, 698 (2020).
[41] K. Jusufi, P. Channuie, and M. Jamil, Eur. Phys. J. C **80**, 127 (2020).
[42] K. Jusufi, S. K., M. Azreg-Aïnou, M. Jamil, Q. Wu, and C. Bambi, arXiv:2106.08070.
[43] C. Bambi, Phys. Rev. D **87**, 107501 (2013).
[44] C. Bambi and D. Stojkovic, Universe **7**, 136 (2021).
[45] D. C. Dai and D. Stojkovic, Phys. Rev. D **100**, 083513 (2019).
[46] D. C. Dai, D. Minic, and D. Stojkovic, Eur. Phys. J. C **80**, 1103 (2020).
[47] J. H. Simonetti, M. J. Kavic, D. Minic, D. Stojkovic, and D. C. Dai, Phys. Rev. D **104**, L081502 (2021).
[48] R. Shaikh and P. S. Joshi, J. Cosmol. Astropart. Phys. 10 (2019) 064.
[49] C. Liu, T. Zhu, and Q. Wu, Chin. Phys. C **45**, 015105 (2021).
[50] C. Liu, S. Yang, Q. Wu, and T. Zhu, arXiv:2107.04811.
[51] G. Gyulchev, P. Nedkova, T. Vetsov, and S. Yazadjiev, Eur. Phys. J. C **81**, 885 (2021).
[52] G. Gyulchev, J. Kunz, P. Nedkova, T. Vetsov, and S. Yazadjiev, Eur. Phys. J. C **80**, 1017 (2020).
[53] G. Gyulchev, P. Nedkova, T. Vetsov, and S. Yazadjiev, Phys. Rev. D **100**, 024055 (2019).
[54] T. Harko, Z. Kovacs, and F. S. N. Lobo, Phys. Rev. D **78**, 084005 (2008); Classical Quantum Gravity **26**, 215006 (2009).
[55] A. Simpson and M. Visser, J. Cosmol. Astropart. Phys. 02 (2019) 042.
[56] J. Mazza, E. Franzin, and S. Liberati, J. Cosmol. Astropart. Phys. 04 (2021) 082.
[57] E. Franzin, S. Liberati, J. Mazza, A. Simpson, and M. Visser, J. Cosmol. Astropart. Phys. 07 (2021) 036.
[58] N. Tsukamoto, Phys. Rev. D **104**, 064022 (2021).
[59] K. A. Bronnikov, R. A. Konoplya, and T. D. Pappas, Phys. Rev. D **103**, 124062 (2021).
[60] R. Shaikh, K. Pal, K. Pal, and T. Sarkar, Mon. Not. R. Astron. Soc. **506**, 1229 (2021).
[61] N. Tsukamoto, Phys. Rev. D **103**, 024033 (2021).
[62] F. S. N. Lobo, M. E. Rodrigues, M. V. d. S. Silva, A. Simpson, and M. Visser, Phys. Rev. D **103**, 084052 (2021).
[63] Z. Stuchlík and J. Vrba, Universe **7**, 279 (2021).
[64] M. Guerrero, G. J. Olmo, D. Rubiera-Garcia, and D. S. C. Gómez, J. Cosmol. Astropart. Phys. 08 (2021) 036.
[65] Z. Younsi, A. Zhidenko, L. Rezzolla, R. Konoplya, and Y. Mizuno, Phys. Rev. D **94**, 084025 (2016).
[66] C. Bambi, Astrophys. J. **761**, 174 (2012).
[67] M. Ghasemi-Nodehi, Eur. Phys. J. C **80**, 405 (2020).